

## Preliminary Pulsed Phase Thermography analysis on cylindrical geometry

by L. Salvi, L. Vitali, D. Fustinoni, P. Gramazio and A. Niro

Politecnico di Milano, Energy Department, Via Lambruschini 4, 20156 Milano, Italy,  
 alfonso.niro@polimi.it

### Abstract

This work is aimed at characterizing internal flaws in cylindrical geometry using the Pulsed Phase Thermography (PPT). A preliminary experimental evaluation of the emissivity variations as well as of the out-of-focus effects due to non planar shape has been preliminary performed, then a procedure to compensate for these non-uniformities has been implemented and experimentally tested on a hollow emicylindrical Plexiglas pipe section with dummy holes. The defect depth retrieval method is based on a phasegram correlation analysis.

### 1. Introduction

Since the first paper of Maldague and Marinetti [1], Pulsed Phase Thermography (PPT) has been proved to be a powerful concept for the non destructive testing (NDT) of a wide range of materials. Despite this fact, many issues arise when this technique is used in specific applications, especially about the analysis and interpretation of thermographic sequence, or its Fourier transform. In particular, industrial pipelines are an important field of application of NDT techniques, and various specific studies on this subject can be found in the open literature [2-4].

In this paper, some preliminary experiments have been carried out to evaluate how a variation of specimen orientation affects the test, taking into account directional emissivity, out-of-focus effects and uneven thermal excitation; then this knowledge is applied in a test of a hollow emicylindrical (half pipe) polymethylmethacrylate sample, analyzed with the depth retrieval procedure developed in our laboratory.

### 2. Pulse Phase Thermography

Let us suppose to heat a specimen with a thermal pulse generated by an external source, like a flash or a lamp, and then to collect a sequence of the temperature fields on the excited face by means of an IR-camera. If there is a defect inside the specimen, a hot spot will appear on the surface above that. The thermogram sequence may be analyzed as it is, i.e., as a temporal evolution of the temperatures, and the related processing procedures are called *time domain techniques*, or it may be Fourier-transformed commuting consequently from the temperature-time variables to the phase-frequency or amplitude-frequency variables, speaking in this case of *frequency domain techniques*. The PPT uses the couple of variables phase-frequency, and formally it can be summarized as

$$\varphi(\vec{r}, f) = \arg\{\mathfrak{F}[\tilde{T}(\vec{r}, t)]\} \quad (1)$$

where  $\mathfrak{F}$  stands for the Fourier transform,  $T(\vec{r}, t)$  is the temperature distribution at the time  $t$  on the specimen surface that is thermally excited ( $\vec{r}$  is the position vector), and  $\varphi(\vec{r}, f)$  the phase distribution on the same surface at the frequency  $f$ . Because from a practical point of view the specimen surface temperature is known as a discrete function of  $\vec{r}$  and  $t$ , no matter whether experimentally measured or numerically calculated, the Fast Fourier Transform (FFT) algorithm is indeed used, and the discrete version of the PPT procedure can be conceptually schematized as in figure 1.

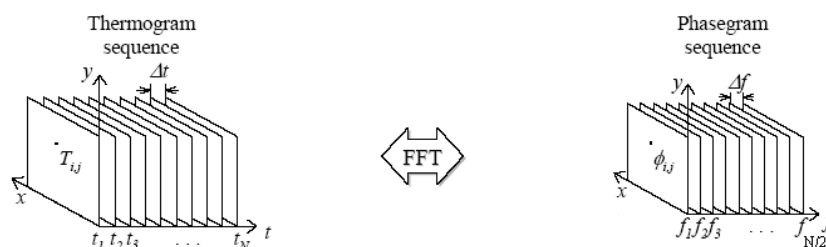


Fig. 1. Pulse Phase Thermography, conceptual scheme (adapted from [8]).

The purpose of this operation is to emphasize the eventual presence of subsurface defects and to characterize their geometrical properties, especially their depth, by associating the frequencies of the resulting phase images, or phasegrams, to the diffusion length of the thermal pseudo-waves.

### 3. Experiments

#### 3.1. Experimental setup

The experimental setup for the PPT test, as schematically shown in figure 2, comprises basically an IR camera, a thermal stimulation apparatus, and the specimen. The IR camera is a Raytheon Radiance HS (InSb, Focal Plane Array, detectable wavelength range 3-5  $\mu\text{m}$ ). The thermal stimulation apparatus consists of two reflectors, each one equipped with a 500W halogen lamp and a guillotine shutter in order to ensure a thermal square pulse to a good extent. The specimen is a polymethylmethacrylate (PMMA), 150 mm external diameter, 10 mm thick and 200 mm high hollow cylinder, whose thermal properties relevant to the experiment are listed in table 1. The specimen outer side, i.e. the thermally excited one, is blackened to enhance its emissivity, whereas on the internal side several flat-bottomed holes are drilled to simulate the defects. It is worth remarking that defect detection relies upon thermal wave reflection, that is a phenomenon localized at the interface between material and defect, and thus it depends on the reflection coefficient  $\hat{r}$  but it is completely independent of the defect thickness, so that a drilled hole is equivalent to a subsurface crack.

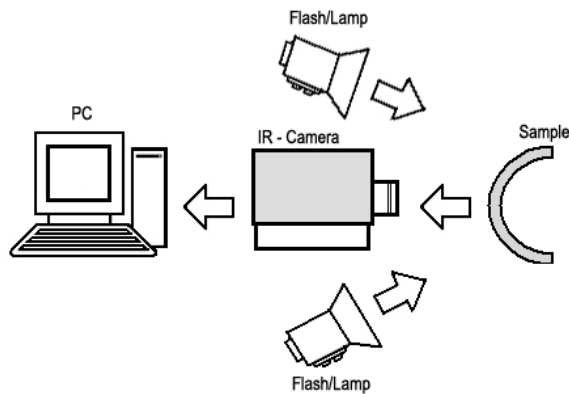


**Fig. 2.** Scheme of the experimental setup

**Table 1.** Thermal properties of specimen material (PMMA)

|                                    |                                     |       |
|------------------------------------|-------------------------------------|-------|
| Density                            | $\rho$ [ $\text{kg}/\text{m}^3$ ]   | 1190  |
| Specific heat at constant pressure | $c$ [ $\text{J}/(\text{kg K})$ ]    | 1470  |
| Thermal conductivity               | $k$ [ $\text{W}/(\text{m K})$ ]     | 0.19  |
| Thermal diffusivity                | $\alpha$ [ $\text{mm}^2/\text{s}$ ] | 0.109 |

#### 3.2. Directional emissivity

When dealing with non-planar specimens, we need to preliminarily measure the directional total emissivity sensed by the IR-camera. In order to do that, a 460 mm x 100 mm x 20 mm rectangular aluminium channel has been externally black-painted with the same paint used for the surface coating of the specimens, and its two ends have been connected to a heating circulator (**Thermo** Haake P2-B12) so that a constant temperature water flow can pass through it lengthwise, as shown in figure 3. The temperature set-point of the heating circulator is 41.5°C, a temperature comparable to those reached by the PPT sample after the thermal stimulus, and higher enough than ambient temperature in order to minimize the errors caused by ambient IR reflections. The IR camera has been calibrated in-situ to obtain accurate temperature measurements for the adopted black paint, as reported in [5]. Its integration time is set at 0.25 s, so that the temperature sensitivity in the 40-45°C range is 0.06°C. A type T miniaturized thermocouple, that has been calibrated in the same water circulator with a PT100 as reference, is cemented in a groove cut into the box surface, in order to measure the actual surface temperature. When the sample reaches a steady-state temperature condition, i.e. the fluctuations of the thermocouple measurements are within  $\pm 0.02^\circ\text{C}$ , 700 IR images at a frame rate of 10 Hz are collected for each considered observation angle  $\theta$  (0°, 30°, 45°, 60°, 75°). A time-average and a mean filter are then successively applied to the thermogram sequence, and one single value of temperature per orientation, as listed in table 2, is extracted by final spatial average on the resulting thermal image.

**Table 2.** IR Camera averaged readings for tilted specimen

| $\theta$      | 0°    | 30°   | 45°   | 60°   | 75°   |
|---------------|-------|-------|-------|-------|-------|
| <b>T [°C]</b> | 41.49 | 41.33 | 41.20 | 40.81 | 39.39 |

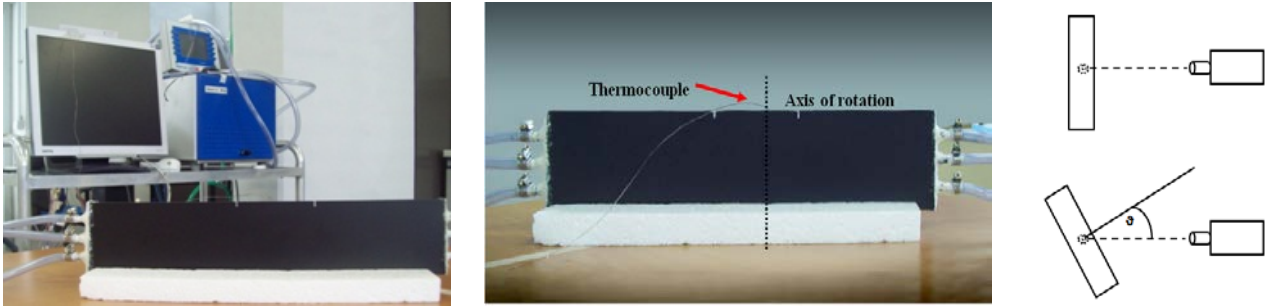


**Fig. 3.** Experimental setup for directional emissivity measurements

Neglecting reflections (ambient or from other sources), the emissive power of the specimen, that is proportional to the IR-camera reading, is

$$W(\theta) = \sigma \varepsilon(\theta) \bar{T}_r^4 \quad (2)$$

Where  $\bar{T}_r$  is the actual average sample temperature. However, the angular dependence of the IR-camera readings can be viewed as caused by an angular variation of temperature:

$$W(\theta) = \sigma \varepsilon_0 \bar{T}_m(\theta)^4 \quad (3)$$

where  $\bar{T}_m$  is the average temperature of the specimen measured by the IR-camera. Being  $\varepsilon_0 = \varepsilon(\theta=0^\circ)$  the emissivity value determined by the in-situ calibration,

$$\begin{aligned} \varepsilon(\theta) \bar{T}_r^4 &= \varepsilon_0 \bar{T}_m(\theta)^4 \\ \varepsilon(\theta = 0^\circ) \bar{T}_r^4 &= \varepsilon_0 \bar{T}_m(\theta = 0^\circ)^4 \end{aligned} \quad (4)$$

The angular dependency of the relative-to-normal emissivity can be expressed as the ratio (4)

$$\varepsilon_r(\theta) = \frac{\bar{T}_m(\theta)^4}{\bar{T}_m(\theta = 0^\circ)^4} \quad (5)$$

The relative emissivity values, as determined with equation 5, are shown in figure 4. Due to the steep decrease of emissivity values after  $\theta = 60^\circ$ , IR measurements are considered reliable only for inclination angles within the range  $0^\circ - 60^\circ$ .

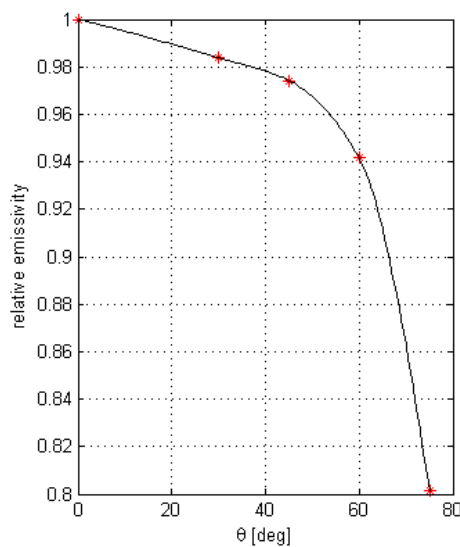


**Fig. 4.** Angular variation of relative-to-normal emissivity

### 3.3. Out-of-focus effects

Beside the inevitable blurring and loss of definition of thermogram regions that are slightly out-of-focus due to the different distance from the IR camera lens, an evaluation has been made on possible alterations of the temperature field due to this effect.

To do so, the same experimental apparatus and image acquisition procedure described in paragraph 3.2 is used. The IR camera is focused on the rotation axis. For each observation angle  $\theta$ , the standard deviation of the temperature measurement has been calculated for an increasing width of a pixel column centered on the rotation axis (15, 21 and 31 pixels, respectively equivalent to 13.5, 18.9 and 27.9 mm). Even at the higher angle ( $\theta=75^\circ$ ), the measurement standard deviation is comparable to the sensitivity of the instrument, so it is assumed that the out-of-focus effect does not alter the temperature measurement.

**Table 3:** standard deviations of T, 31 pixel (27.9 mm) column width

| $\theta$ [°]                           | 30   | 45   | 60   | 75   |
|--|------|------|------|------|
| <b>max <math>\sigma(T)</math> [°C]</b> | 0.06 | 0.07 | 0.07 | 0.11 |

### 3.4. Experimental post-processing stage

After having acquired the thermogram sequence of the PPT trial, the post-processing stage starts with the conversion from grayscale values to temperature values. The sequence is then cut and centered so as to display only the region of interest, and to speed up the procedures presented in the following sections.

#### 3.4.1. Emissivity evaluations and filtering

A correction procedure has been implemented in order to take into account the emissivity variations caused by the curvature of the specimen, that without surprise shows higher readings when the surface normal vector points towards the IR-camera with a small angle. To identify the view angle on the thermogram sequence, a routine that associates a geometric model of the sample to the pixel position has been implemented. The temperature values are then corrected by applying the angular variation of the emissivity to the temperature field.

After this stage, the FFT algorithm is applied to the thermogram sequence, hence obtaining the phasegram sequence, to whom a mean and a gaussian filter (with 3x3 pixel mask) are applied.

#### 3.4.2. Phasegram correlation method

By observing that PPT may be considered as a multi-frequency scanning technique, Gutierrez-Fajardo in [6] argued that for each defect there is a frequency at which the defect appears as clear as possible, which he referred as the *optimal visibility frequency*  $f_{opt}$  to, and that the defect depth is strictly proportional to the diffusion length calculated with that frequency. So the multi-frequency analysis is eventually used as a single-frequency analysis.

In order to determine the optimal visibility frequency, Gutierrez-Fajardo proposed maximizing the (discrete) function given by the correlation coefficients between pairs of successive phasegrams for the whole sequence. More precisely, by considering the IR-image taken at the time instant  $t_k$ , with  $k$  ranging between 1 and N, a rectangle of AxB pixels with coordinates  $i$  and  $j$ , as shown in Fig. 1, let  $[\Phi_k]$  be the matrix associated to the phasegram at the frequency  $f_k$  corresponding to the instant  $t_k$ , whose elements are

$$\tilde{\phi}_{ij}(f_k) = \tilde{\varphi}(r_{i,j}, f_k) = \text{arg}\{FFT[\tilde{T}_{ij}(t_k)]\} \quad (6)$$

where  $\tilde{T}_{ij}(t_k) = \tilde{T}(r_{i,j}, t_k)$ . The correlation coefficient between two successive phasegrams is calculated by

$$\hat{r}([\Phi_k], [\Phi_{k+1}]) = \frac{\sum_{i=1}^A \sum_{j=1}^B (\phi_{ij}(f_k) - \bar{\phi}_k)(\phi_{ij}(f_{k+1}) - \bar{\phi}_{k+1})}{\sqrt{\left[\sum_{i=1}^A \sum_{j=1}^B (\phi_{ij}(f_k) - \bar{\phi}_k)^2\right] \left[\sum_{i=1}^A \sum_{j=1}^B (\phi_{ij}(f_{k+1}) - \bar{\phi}_{k+1})^2\right]}} \quad (7)$$

where

$$\bar{\phi}_k = \frac{1}{AB} \left[ \sum_{i=1}^A \sum_{j=1}^B \phi_{ij}(f_k) \right] \quad (8)$$

Then, with the values of the correlation coefficient obtained for each pair of consecutive phasegrams of the whole sequence, the following (discrete) function may be constructed

$$\tilde{R}(f_k) = [\hat{r}([\Phi_1], [\Phi_2]), \hat{r}([\Phi_2], [\Phi_3]), \dots, \hat{r}([\Phi_k], [\Phi_{k+1}]), \dots, \hat{r}([\Phi_{N/2-1}], [\Phi_{N/2}])] \quad (9)$$

According to Gutierrez-Fajardo, the frequency that maximizes the function  $\tilde{R}(f_k)$  is the optimal visibility frequency  $f_{opt}$  (being two frequencies at once considered, he proposed to keep as  $f_{opt}$  the lowest of the two for the first five pairs of phasegrams, and their mean value for the other pairs).

Finally, the defect depth is proportional to the diffusion length calculated with the optimal visibility frequency

$$z_{def} = C_1 \tilde{\mu}(f_{opt}) = C_1 \sqrt{\frac{\alpha}{\pi f_{opt}}} \quad (10)$$

where  $C_1$  is a constant depending to some extent on the specimen material, that hence has to be experimentally determined.

In the presented test, the value of  $C_1$  is calculated by the simulation program presented in [7] and has been experimentally validated on 20 mm and 4 mm thick Plexiglas planar specimens with flat-bottomed holes: its value is 1.15.

#### 4. Results

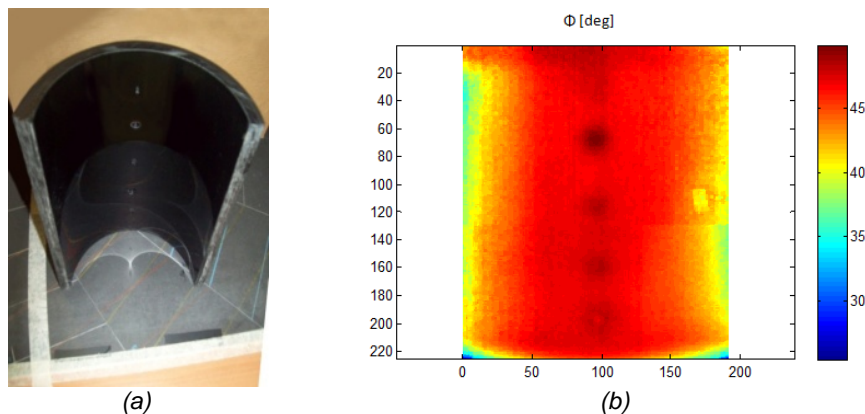


Fig. 5. Specimen (a), phasegram,  $f = 1.7$  mHz (two images montage) (b)

The first experimental results, as listed in table, are relative to the frontal view of the flaws. The only defect whose depth cannot be identified by the adopted procedure is the smallest one (2 mm diameter, 2 mm depth).

Table 4. Experimental results, frontal view

| Diameter [mm] | Depth [mm] | Estimated depth [mm] | Error |
|---------------|------------|----------------------|-------|
| 2             | 2          | -                    | -     |
| 8             | 5          | 4.6                  | 8%    |
| 4             | 5          | 4.6                  | 8%    |
| 8             | 8          | 6.5                  | 19%   |
| 4             | 2          | 2.5                  | 25%   |

Where

$$\text{percentage error} = \left| \left( 1 - \frac{\text{Estimated depth}}{\text{Real depth}} \right) * 100 \right| \quad (11)$$

The experimental procedure, as presented in [7], shows a good defect detection capability, but the depth retrieval error can vary depending on the depth of the defect.

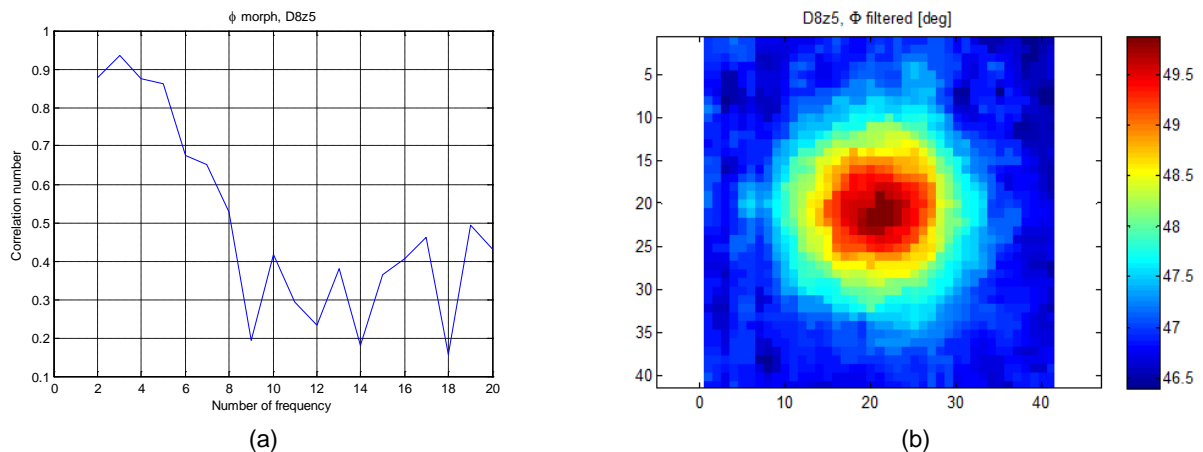


**Fig. 6:** Correlation number vs. Frequency number (a), phase image of a 8 mm diameter and 5 mm depth defect (b)

## 5. Conclusions

In this paper some preliminary analyses for the non-destructive testing of non-planar specimens by PPT have been presented. In particular, the angular emissivity variation test has been used to correct the temperature values for surface inclinations with respect to the IR-camera lower than 60°. Larger inclinations show a quick decrease of the emissivity values.

The PPT preliminary test confirms the capability of the adopted post-processing procedure, based on the phasegram correlation, to retrieve the defect depth.

Further developments of these experiments consider the application of the PPT on pipe segments, that can be ideally analyzed with three PPT tests, especially for defect typologies that are the most common failure cause in pipe segments.

## REFERENCES

- [1] Maldague X., Marinetti S., "Pulse phase infrared thermography". J. Appl. Phys. 79 (5), 1996.
- [2] Maldague X., "Pipe inspection by infrared thermography", Materials Evaluation 57, 899-902, 1999
- [3] Mayr G., Dietermayr B., Hendorfer G., Sekelja J., "Characterization of defects in curved CFRP samples using Pulsed Thermography and 3D Finite Element simulation", proc. QIRT 2008
- [4] Souza M. P.V., Rebello J. M. A., Soares S. D., Freitas G. A. C., "Defect detection in fiberglass reinforced epoxy composite pipes reproducing field inspection conditions", proc. QIRT 2008
- [5] Fustinoni D., "Analisi della convezione forzata su superfici variamente strutturate", Ph.D. thesis, Politecnico di Milano, 2012
- [6] A. Gutierrez Fajardo A., "An analytical and experimental study on defect recognition methodologies with Pulse Phase Thermography", M.S. thesis, Politecnico di Milano, 2005
- [7] Vitali L., Fustinoni D., Gramazio P., Niro A., "Estimation of trial parameters for Pulse Phase Thermography with low power heat sources", Journal of Phys. Conf. Series 501, 2014
- [8] Ibarra Castanedo, C., "Quantitative subsurface defect evaluation by pulsed phase thermography: depth retrieval with the phase", Ph.D. Thesis, Université Laval, 2005